Hindawi Publishing Corporation
International Journal of Chemical Engineering
Volume 2015, Article ID 485463, 9 pages
http://dx.doi.org/10.1155/2015/485463

Research Article

Fe(III)/TiO_2-Montmorillonite Photocatalyst in Photo-Fenton-Like Degradation of Methylene Blue

Is Fatimah,[1] Iwan Sumarlan,[2] and Tuty Alawiyah[2]

[1]*Chemistry Department, Islamic University of Indonesia, Kampus Terpadu UII, Jalan Kaliurang Km 14 Sleman, Yogykarta 55581, Indonesia*
[2]*Chemistry Department, Mataram University, Nusa Tenggara Barat 55584, Indonesia*

Correspondence should be addressed to Is Fatimah; isfatimah@uii.ac.id

Received 19 February 2015; Revised 4 May 2015; Accepted 4 May 2015

Academic Editor: Xijun Hu

A photodegradation process of methylene blue (MB) in aqueous solution using Fe(III)/TiO_2-montmorillonite photocatalyst is presented. The photocatalyst material was prepared using Indonesian natural montmorillonite in TiO_2 pillarization process followed by Fe(III) ion exchange. Kinetic study on MB degradation was conducted and evaluated by three kinetic models: the pseudo-first- and second-order equations and the Elovich equation. From the results, it is concluded that the degradation under the photo-Fenton-like process utilizing Fe(III)/TiO_2-montmorillonite photocatalyst conformed to the Elovich kinetic model.

1. Introduction

Dye removal from wastewater is a main problem encountered in the textile industry. Color is caused by visible dying pollutants, which are organic compounds blocking light and inducing toxicity, and therefore it is required that the organic contaminants in effluents be treated before the effluents are discharged into an aquatic environment [1]. In this field of research, a novel technology to remove the contaminants by Advance Oxidation Processes (AOPs) using a photo-Fenton-like process has been widely developed [2, 3]. Photocatalysis utilizing titanium dioxide (TiO_2) has gained great interest due to not only its high photocatalytic activity, chemical stability, and low cost but also its band gap energy (anatase, 3.2 eV) permissible for UV excitation obtained from the solar spectrum. Furthermore, in the photo-Fenton-like process, the combination of Fe^{3+} with TiO_2 is an alternative process that can be operated in an effective, easy to control, and also cost-efficient manner [4, 5]. Some efforts concerned with modification of the photo-Fenton catalyst with some inorganic supports have been reported. Apart from its advantages in minimizing the cost of the process due to the reusability properties, a more efficient heterogeneous photocatalytic process can be gained in a supported photocatalyst with adsorption on the porous support [6, 7]. A wide range of solid materials, such as ZSM-5, silica, transition metal exchanged-zeolites, and pillared clays, have been reported to be active in oxidative degradation of organic compounds involved in dye compounds through the photo-Fenton-like reaction [8]. Some minerals such as hematite, goethite, and vermiculite and also activated carbon were reported to be iron ions to give more effective photocatalysis during the oxidation process [9]. This offers an interesting advantage for its application on an industrial scale; that is, photocatalysts can be reused and can be stable in a wide range of pH.

As investigated in previous works, the reuse of a photocatalyst based on clay materials as a support is in line with the synergistic effect of the adsorptive properties of the support [10, 11]. This work investigated a commonly used dye model: methylene blue (MB). The investigation focused on a kinetic study of degradation which occurred in the adsorption and photodegradation process. The effects of pH and H_2O_2 addition as oxidants in the system were also considered. Referred investigation was the combined Fe(III) with TiO_2 photocatalyst that has higher photoactivity through wider range of light absorbability in visible region [12]. By the combination of pillared montmorillonite porous structure, prepared material was hypothesized to be more

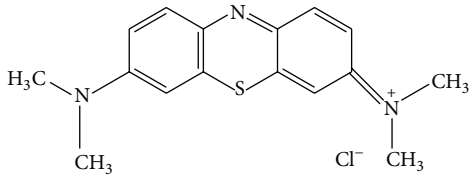

Figure 1: Structure of methylene blue.

effective and ecofriendly heterogeneous photocatalyst for dye photodegradation in water.

2. Materials and Method

The montmorillonite used in this study was obtained from Tunas Inti Makmur PT, Semarang, Indonesia. Iron sulphate dihydrate and titanium isopropoxide as metal precursors of Fe and TiO_2 were supplied by E Merck. As a target molecule, methylene blue with a molecular formula of $C_{16}H_{18}N_3SCl$ and molecular weight of 319.85 g/mol was used. It was chosen as a simple model of a series of common azo dyes widely used in the industry, and its structure is reported in Figure 1.

Preparation of Fe/Ti-montmorillonite photo-Fenton-like catalyst was conducted by TiO_2 pillarization of montmorillonite (Ti-MMT) followed by Fe^{3+} ion exchange (Fe/Ti-MMT). Based on the structure of montmorillonite with tetrahedral silicate and octahedral aluminate at 2 : 1 ratio, titanium pillarization creates porous titania as a pillar between the two units of silica-alumina layers [13–15]. The prepared pillared clay still has exchangeable cations to accommodate iron ions.

Solution of titanium isopropoxide in isopropanol solvent was used as titanium source. The precursor solution was dispersed into montmorillonite suspension to get Ti theoretical content of 10% wt. The mixture was then stirred for 4 h before it was filtered, dried for overnight, and calcined at 400°C for 4 h. Solid material obtained from these steps was encoded as Ti-MMT. For Fe/Ti-MMT preparation the solid of Ti-MMT was dispersed in mixture with $FeCl_3$ solution followed by stirring for 24 h. The concentration of Fe^{3+} was 5 times cation exchange capacity (CEC) of Ti-MMT (45 meq/100 g). For comparison purpose, preparation of Fe-MMT was also conducted by ion exchange method. Ion exchange was engaged by mixing MMT powder in $FeCl_3$ solution at Fe theoretic content equal to 5 times CEC of MMT (69 meq/100 g). The chemical composition and physicochemical characteristics of montmorillonite and prepared materials were investigated by X-ray diffraction (XRD) analysis, surface area, and porosity analysis by gas sorption analyzer NOVA 1200e, scanning electron microscope-energy dispersive X-ray fluorescence (SEM-EDX) JEOL, and FTIR analysis. The XRD patterns of materials were obtained by packing finely ground samples into an aluminium sample holder and scanned from 2 to 60° of 2θ at a rate of 2°/min. A Shimadzu X6000 diffractometer with a Ni-filtered Cu-Kalpha was used. Surface parameters consisting of Brunair-Emmet-Teller (BET) specific surface area, pore radius, and pore volume were calculated based on N_2 adsorption-desorption analysis using gas sorption analyzer.

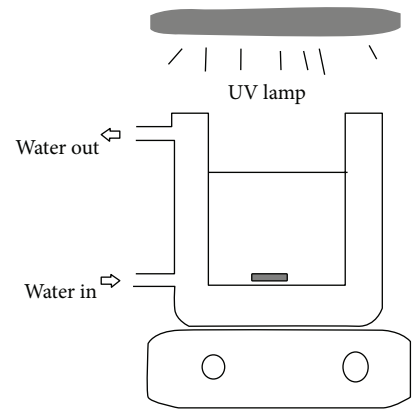

Figure 2: Scheme of photodegradation reactor.

For the experiment of the photo-Fenton-like process, a photocatalyst was charged into the solution of MB in various initial concentrations under UVB lamp exposure and stirred. A scheme of the reactor is presented in Figure 2.

The degradation/decolorization was observed via UV-Visible spectrophotometric analysis (HITACHI U2010) and high performance liquid chromatography (Shimadzu) for determination of MB concentration and detection of oxidation products. The dynamic MB degradation was analyzed by three kinetic models, the pseudo-first- and second-order equations and the Elovich equation. Kinetic parameters, rate constants, equilibrium adsorption capacities, and correlation coefficients, for each kinetic equation, were calculated and discussed. The experimental isotherm data were analyzed using the Langmuir, Freundlich, and Temkin equations.

3. Results and Discussion

3.1. Material Characterization. XRD patterns of the prepared materials are presented in Figure 3.

From the reflections, all samples exhibit strong diffraction peak at 5.9° indicating basal spacing [001] of montmorillonite and other peaks at 19.89° and 35.6° corresponding to [020] and [006] reflections. Compared to MMT, the formation of titanium dioxide pillar in the Ti-MMT is indicated by the shift of [001] reflection to the lower angle corresponding to the increasing d001. The pillar of TiO_2 in the interlayer space of silica-alumina layers was formed. Other peaks at 25° and 27° correspond to the anatase [101] and the rutile [110], respectively, showing two phases of TiO_2 in the prepared material. The formation of anatase and rutile form of TiO_2 exhibits that the calcination over Ti-intercalated montmorillonite converts the ionic form into oxide form. After Fe(III) dispersion, the [001] reflection at around 5.9° of Ti/MMT is maintained with lower intensity that expressed the reduced crystallinity. Moreover the presence of Fe(III) in Fe/Ti-MMT is not clearly described as no specific reflection is responsible for Fe oxide formation of the sample. This is related to the fact that Fe attachment in the Ti-MMT is performed by

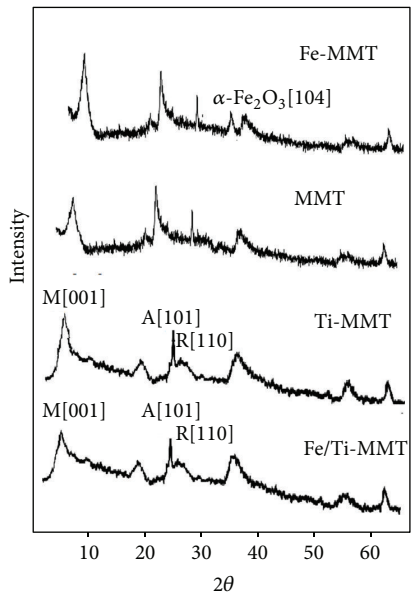

Figure 3: XRD pattern prepared material compared to raw MMT.

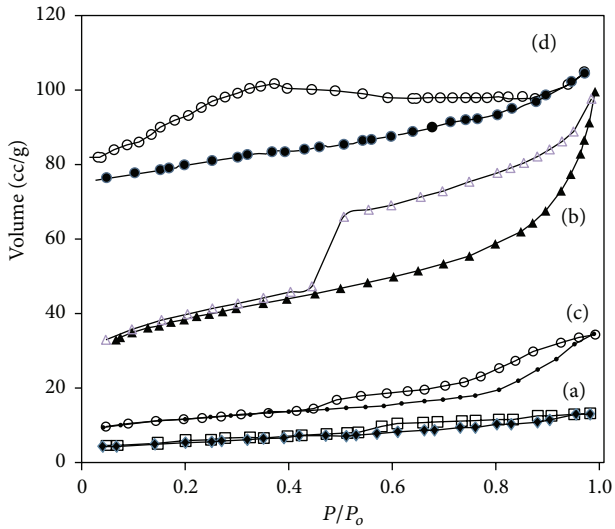

Figure 4: Adsorption-desorption profile of (a) MMT, (b) Ti-MMT, (c) Fe/Ti-MMT, and (d) Fe-MMT.

ion exchange mechanism so there is no oxide formation of Fe(III) during the synthesis. The result ionic form of Fe^{3+} ions are required in the Fenton-like mechanism. For Fe-MMT, there is specific reflection at around 36° corresponding to the formation of α-Fe_2O_3 [16]. The formation of α-Fe_2O_3 is probably caused by pillarization mechanism that is included within the process [17].

The important physicochemical characteristics of the materials are revealed by elemental analysis and N_2 adsorption-desorption analysis for specific surface area, pore volume, and pore radius calculation depicted in Figure 4 and data are listed in Table 1. Prepared material Fe/Ti-MMT contains Fe of 2.48 wt.% and Ti of 10.95 wt.%. The contents of SiO_2 in the range of 40.56–46.52 wt.% and Al_2O_3 of 23.25–27.95 wt.% show the Si/Al ratio at 2–2.25, an indication of the main content of the parent material montmorillonite [18]. The specific surface area is 120 m^2/g, and pore volume and pore radius are 0.152 cc/g and 15 Å, respectively. Compared to Fe content in Fe/Ti-MMT, the content in Fe-MMT is much higher (8.16% wt.) because the exchange process was conducted in higher concentration considering the higher CEC value in MMT than in Ti-MMT. It is also noted that specific surface area of Fe-MMT is the highest (205.38 m^2/g).

FTIR analysis (Figure 5) shows major bands of the montmorillonite as phyllosilicate backbone in the range of 470–1120 cm^{-1}. These bands are associated with Si-O-Si and Si-O-Al bending and stretching vibrations. The band at 1042.9 cm^{-1} in montmorillonite sample associated with Si-O-Si stretching vibration is shifted to 1048.7 cm^{-1} on Fe/Ti-MMT sample and 1044.88 cm^{-1} for Fe-MMT. The attachment of Fe atom on Si-O bond causes the larger vibration energy. Similar shifts for Al-O-H vibration band at 916.57 cm^{-1} for montmorillonite are occurring at 916.58 cm^{-1}, 920.34 cm^{-1}, and 918.54 cm^{-1} for Ti-MMT, Fe/Ti-MMT, and Fe-MMT samples, respectively, while Si-O bending at 466.62 cm^{-1} of MMT is shifted to 471.2 cm^{-1} for Fe/Ti-MMT sample and 480.22 cm^{-1} for Fe-MMT. It is concluded that the addition of TiO_2 and Fe ions within the crystal structure affects the linkage of Si-O and Al-O bonds. Surface profile of materials is presented in Figure 6. Dispersed TiO_2 appeared on surface of MMT as shown by white particles on surface.

3.2. Photocatalytic Activity. Photocatalytic activity of the material was studied by several procedures. Figure 7 shows the profiles of MB reduction by varied methods: the addition of photocatalyst without UV illumination with and without H_2O_2 addition, as a function of treatment. MB removal is defined by the ratio of the rest of the concentrations at each time (C/C_o). Initial velocity of MB reduction under varied condition is tabulated in Table 2.

Initial rate of MB degradation in each treatment is listed in Table 2.

From the kinetic curve and initial rate data, it can be concluded that actually there is no significant difference between the treatments with and without H_2O_2 addition. The addition of H_2O_2 is as oxidant agent that can be activated by UV light illumination. Photon from UV light can break H_2O_2 into hydrogen peroxide from which then oxidise organic content in the solution. The concentration reduction over those treatments is probably caused by adsorption mechanism. From compared photocatalyst material, it can be seen that the highest rates achieved by Fe-MMT in the initial rates data of MB reduction are linear along the increasing specific surface area. By the adsorption mechanism, the highest initial rate is achieved by Fe-MMT that has the highest specific surface area. Figure 8 and Table 3 demonstrate the kinetic data of treatment with UV illumination with and without H_2O_2 addition.

It is shown that UV illumination has no significant effect on MB removal over MMT. By the addition of H_2O_2 and UV illumination, the initial rates of MB removal catalyzed

Table 1: Physicochemical properties of Fe/Ti-MMT.

Parameter	MMT	Fe/Ti-MMT	Ti-MMT	Fe-MMT
Elemental analysis				
Fe	0.38 (wt. %)	4.14 (wt. %)	0.43 (wt.%)	8.16 (wt.%)
Ti	n.d	10.98 (wt. %)	10.99 (wt.%)	n.d
Al_2O_3	27.09–29.05 (wt.%)	23.25–27.95 (wt. %)	25.67–28.05 (wt.%)	25.70–28.12
SiO_2	49.63–49.21 (wt.%)	40.56–46.52 (wt. %)	42.56–45.59 (wt.%)	43.56–45.59 (wt.%)
Surface analysis				
Specific surface area	69.87 m^2/g	120 m^2/g	198.79 m^2/g	205.38 m^2/g
Pore volume	0.167 cc/g	0.152 cc/g	0.033 cc/g	0.199 cc/g
Pore radius	15.67 Å	15 Å	10.67 Å	12.33 Å

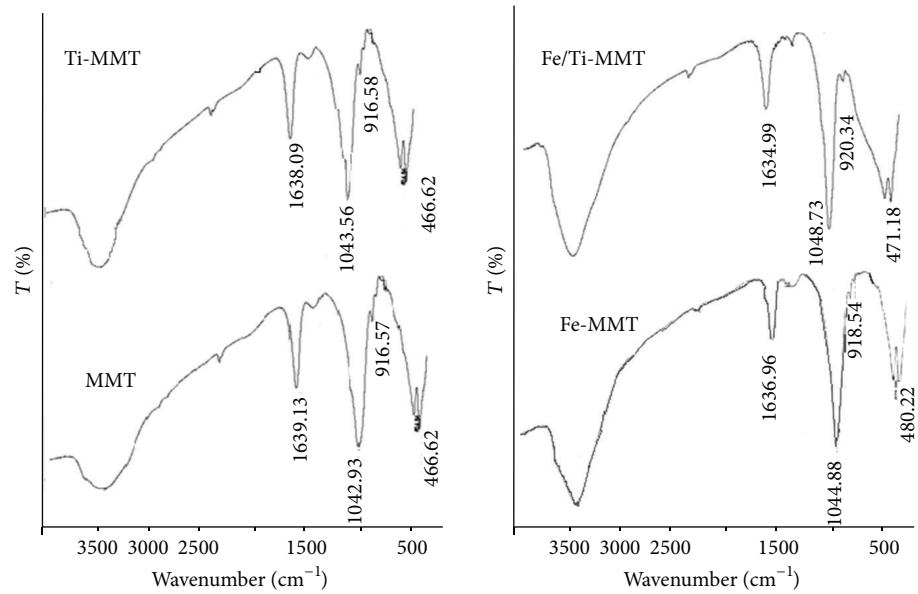

Figure 5: FTIR Spectra of MMT, Ti-MMT, Fe-MMT, and Fe/Ti/MMT.

by Ti-MMT, Fe-MMT, and Fe/Ti-MMT are increased. MB removal reaches 73% for Ti-MMT and Fe-MMT and 80% for Fe/Ti-MMT. Both treatments under UV with and without H_2O_2 addition express the photodegradation mechanism. It is noted that the rate from Fe/Ti-MMT utilization is the highest compared to Ti-MMT and Fe-MMT. H_2O_2 in the presence of UV can produce $^{\bullet}OH$ radicals and other radicals, potentially oxidizing dye molecules in solution [2]. The higher MB removal obtained on Ti-MMT is correlated with the role of TiO_2 as a photoactive semiconductor to accelerate the formation of radicals and superadicals under UV light irradiation. Immobilizing Fe into Ti-MMT gives more and potentially regenerable radicals through the following steps:

$$\mathrm{Fe\,(III)} + \mathrm{H_2O_2} \longrightarrow \mathrm{Fe\,(III)}\left(\mathrm{H_2O_2}\right)_s \quad (1)$$

$$\mathrm{Fe\,(III)}\left(\mathrm{H_2O_2}\right)_s \longrightarrow \mathrm{Fe\,(II)} + \mathrm{HO_2^{\bullet}} + \mathrm{H^+} \quad (2)$$

$$\mathrm{Fe\,(II)} + \mathrm{H_2O_2} \longrightarrow \mathrm{Fe\,(III)} + \mathrm{HO^{\bullet}} + \mathrm{HO^-} \quad (3)$$

When UV light is caught by a photoactive site during UV illumination, the degradation rate of the organic pollutants by the Fenton reaction can increase through the involvement of high valence iron intermediates that are responsible for the direct attack on organic matter. The absorption of light by a complex formed between Fe^{3+} and H_2O_2 is the cause of oxidation and propagation reaction to complete degradation. By comparing Fe/Ti-MMT and Fe-MMT, it is concluded that ionic Fe^{3+} acts as more active Fenton agent while Fe in Fe-MMT is in the oxide form.

The UV-Visible spectra of the dye solution as a function of time (Figure 9) illustrate that there is a different pattern of spectra during the treatment. While the treatment was conducted, the absorption at around 663.5 nm decreased at the longer time, and the presence of new peaks (marked with $*$) at around 260–270 nm after treatment of 180 min appeared. This suggests that the bonds between rings in the MB structure were broken and some aromatic rings were produced by the reaction.

The combination of clay as a support and TiO_2 as a photoactive center provides a synergistic effect, where the clay improves MB adsorption onto the surface before MB being further degraded by radicals formed in the photolysis [19].

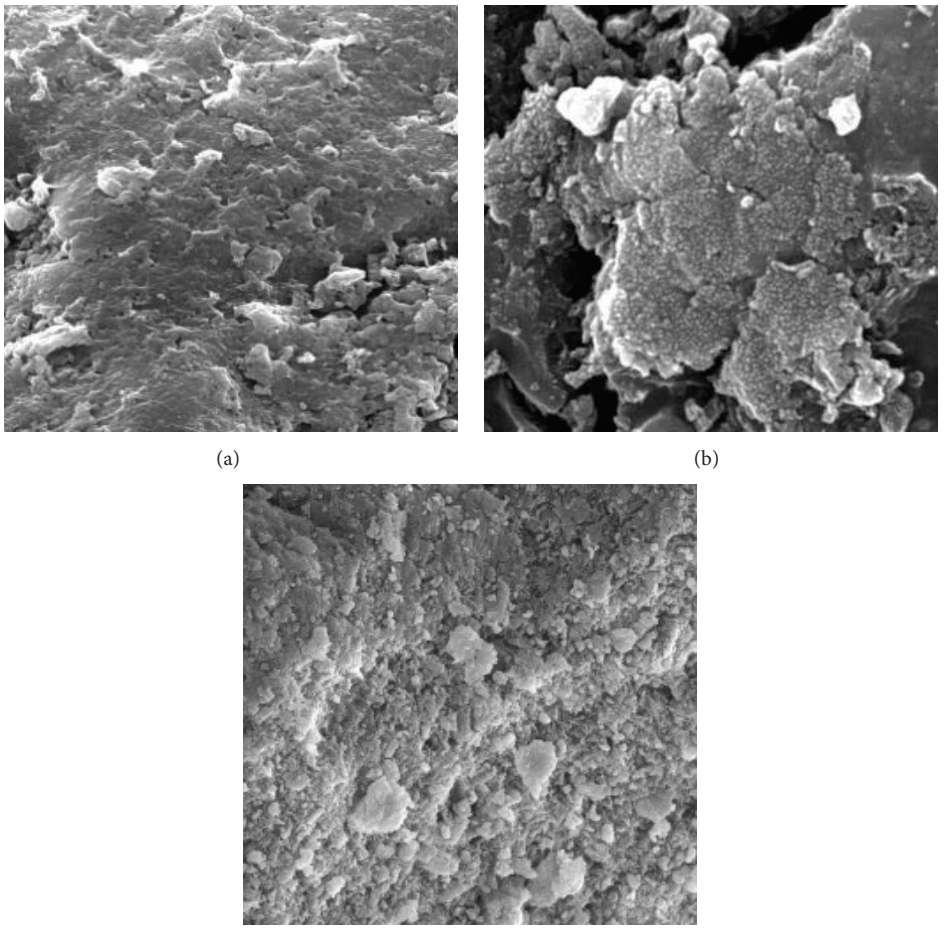

Figure 6: SEM profile of (a) raw montmorillonite, (b) Fe/Ti-MMT, and (c) Fe-MMT.

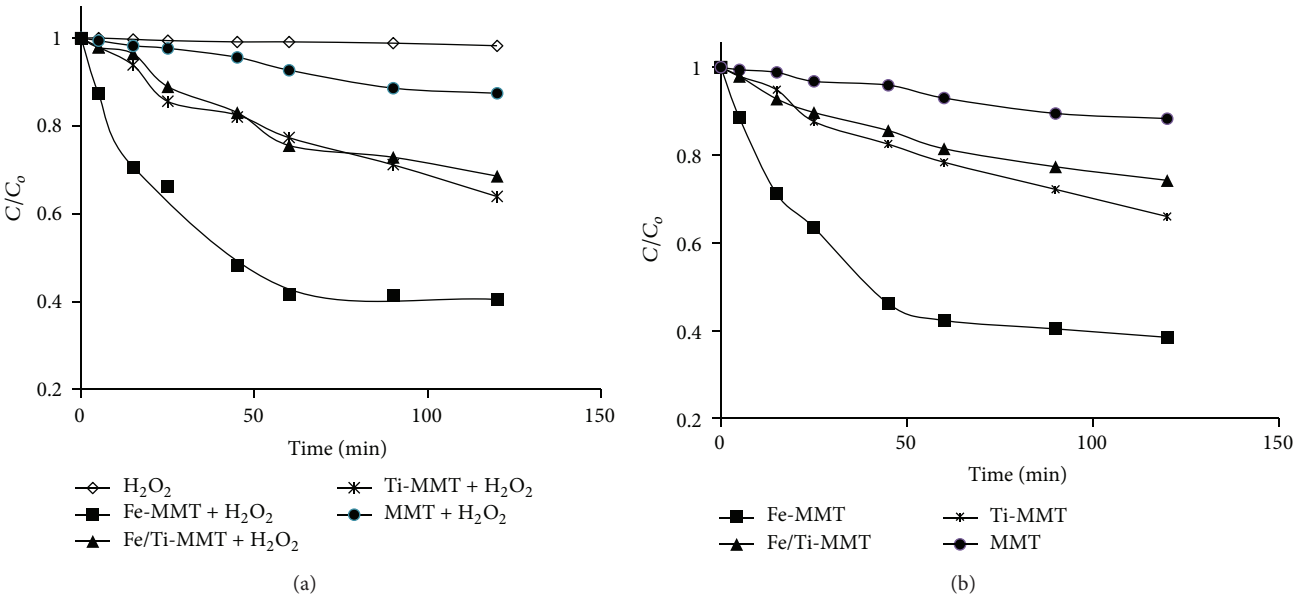

Figure 7: MB removal at varied treatments over photocatalyst without UV: (a) with H_2O_2 addition and (b) without H_2O_2 addition (initial concentration of MB = 5×10^{-4} M).

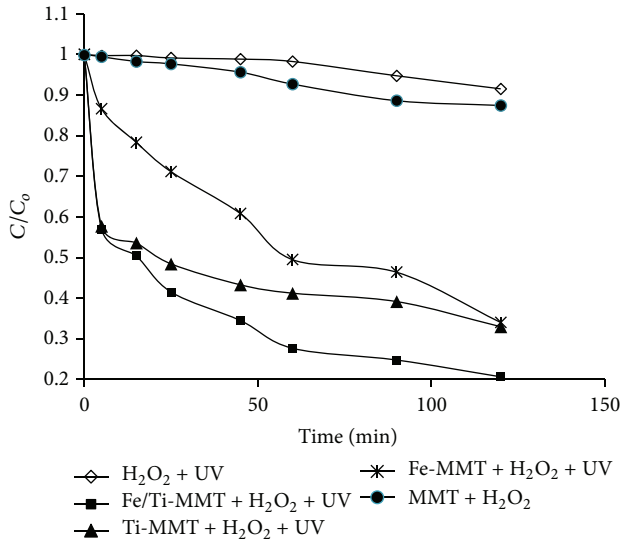

(a)

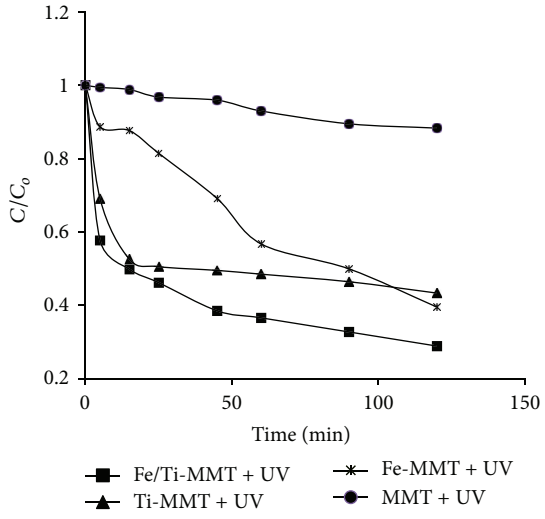

(b)

Figure 8: MB removal at varied treatments over photocatalyst with UV: (a) with H_2O_2 addition and (b) without H_2O_2 addition (initial concentration of MB = 5×10^{-4} M).

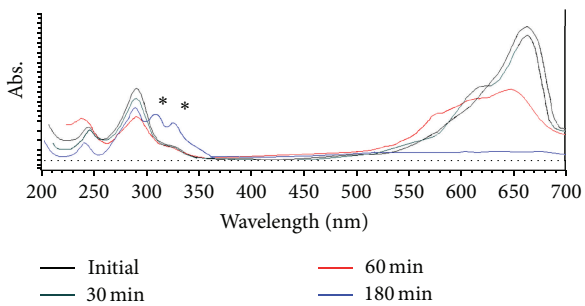

Figure 9: UV-Visible spectra of MB treated solution with Fe/Ti-MMT + H_2O_2 + UV (initial concentration = 5×10^{-4} M).

Table 2: Initial rate of MB degradation by varied treatment without UV.

Treatment	Initial rate (M/s)
H_2O_2	1.97×10^{-7}
Ti-MMT	2.64×10^{-5}
Ti-MMT + H_2O_2	2.95×10^{-5}
Fe/Ti-MMT	2.58×10^{-5}
Fe/Ti-MMT + H_2O_2	2.61×10^{-5}
Fe-MMT	9.75×10^{-5}
Fe-MMT + H_2O_2	9.64×10^{-5}
MMT	6.40×10^{-6}
MMT + H_2O_2	6.47×10^{-6}

Table 3: Initial rate of MB degradation by varied treatment with UV.

Treatment	Initial rate (M/s)
UV + H_2O_2	1.284×10^{-6}
Ti-MMT + UV	1.29×10^{-4}
Ti-MMT + H_2O_2 + UV	1.325×10^{-4}
Fe/Ti-MMT + UV	1.428×10^{-4}
Fe/Ti-MMT + H_2O_2 + UV	1.876×10^{-4}
Fe-MMT + UV	4.89×10^{-5}
Fe-MMT + H_2O_2 + UV	7.33×10^{-5}
MMT + UV	6.46×10^{-6}
MMT + H_2O_2 + UV	6.7×10^{-6}

Furthermore, in order to study the kinetics of MB degradation over Fe/Ti-MMT, treatment at varying initial concentrations of MB was conducted (Figure 10).

Based on the data obtained, pseudo-first-order, pseudo-second-order, and Elovich kinetic models were applied. Both pseudo-first-order and pseudo-second-order models are expressed by the following equations (these models are applied to adsorption, not reaction! Thus, the discussions below are not valid):

$$\log(q_e - q_t) = \log(q_e) - \frac{kt}{2.303}$$
$$\frac{t}{q_t} = \frac{1}{kq_e^2} + \frac{t}{q_e}, \quad (4)$$

where q_e = amount of dyes sorbed at equilibrium (mg/g), q_t = the amount of dyes sorbed at time t (mg/g), and k = rate constant.

Other than both kinetic models, the Elovich model is based on the kinetics of heterogeneous chemisorption of adsorbate in that number of reaction mechanisms including bulk and surface diffusion and activation and deactivation of the catalytic surface are presented. In a solid phase, the expression of the Elovich model is as follows:

$$q_t = \left(\frac{1}{\beta}\right)\ln\left(\frac{\alpha}{\beta}\right) + \left(\frac{1}{\beta}\right)\cdot \ln t, \quad (5)$$

where q_t is the amount of adsorbate per unit mass of adsorbent at time t and α and β are Elovich constant, respectively.

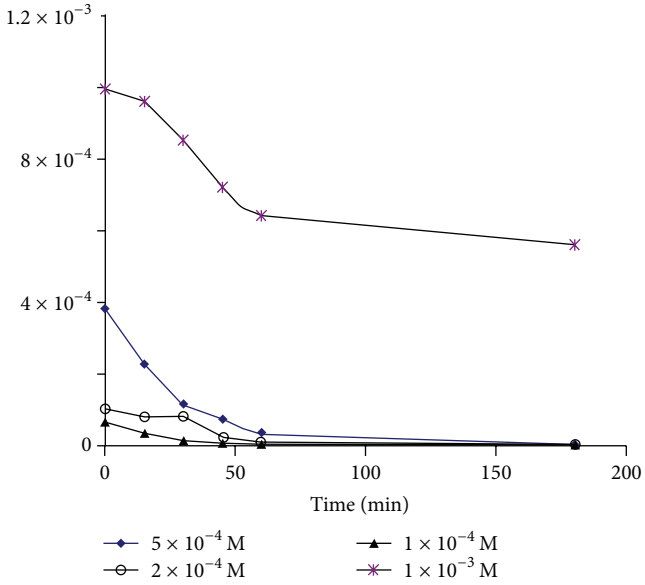

Figure 10: MB degradation rate over Fe/Ti-MMT at varied initial concentration.

Table 4: The fitness kinetics models by determination coefficient (R^2).

MB concentration	Determination coefficient (R^2) of		
	Pseudo-first-order kinetics model	Pseudo-second-order kinetics model	Elovich kinetics model
1×10^{-4}	0.8575	0.9910	0.9672
2×10^{-4}	0.9496	0.8643	0.9503
4×10^{-4}	0.9433	0.8894	0.9804
8×10^{-3}	0.9034	0.8750	0.9993
1×10^{-3}	0.9644	0.8806	0.9956

Based on the equation, the plot of q_t as a function of time of adsorption can be used to determine the α and β constants which express the diffusion efficiency involved in the adsorption mechanism. The plot expresses the condition of Fe/Ti-MMT utilization along with the addition of H_2O_2 as an oxidant and UV as a photon source. It can be noted and understood that the relationship between MB reduction and function time is an exponential function q_s in many kinetics of chemical reaction. Furthermore, the plot was evaluated by three kinds of kinetic models: Elovich kinetics, pseudo-first-order kinetics simulation, and pseudo-second-order kinetics simulation. The fitness of each kinetic model is determined by the determination coefficient (R^2) (Table 4).

From the highest values of the determination coefficient it is concluded that the Elovich model has the best fitness considering that MB degradation by the photo-Fenton-like process utilizing Fe/Ti-MMT photocatalyst obeys the Elovich kinetic model. The expression of MB reduction in the Elovich kinetic model is shown by the curve fitting depicted in Figure 8. The correlation coefficients for the first-order kinetic model obtained at all the studied concentrations were relatively high. The R^2 values for the plots were in the range of 0.950–0.9993. The model suggested that adsorption capability of the photocatalyst is important step in photodegradation mechanism.

Table 5: Initial rate of MB degradation over Fe/Ti-MMT under aerobic and anaerobic condition.

Treatment	Initial rate (M/s)
Aerobic-Fe/Ti-MMT + UV	6.08×10^{-5}
Anaerobic-Fe/Ti-MMT + UV	1.47×10^{-4}
Aerobic-Fe/Ti-MMT + H_2O_2 + UV	9.15×10^{-5}
Aerobic-Fe/Ti-MMT + H_2O_2 + UV	1.42×10^{-4}

3.3. Effect of Aerobic Condition on Photooxidation. Effect of aerobic condition on MB reduction is revealed by the kinetic curve from the experiments of photooxidation and photo degradation over Fe/Ti-MMT presented in Figure 11. The compared experiments are MB reduction over Fe/Ti-MMT catalyst under photocatalysis (without H_2O_2 addition) and photooxidation (with H_2O_2 addition) with O_2 bulbing (aerobic) and N_2 bulbing (anaerobic). Initial rate data are listed in Table 5 [20, 21]. Consider

$$TiO_2 + h\nu \longrightarrow TiO_2\left(e^-_{(CB)} + TiO_2h^+_{(VB)}\right) \quad (6)$$

$$h^+_{(VB)} + H_2O \text{ or } OH \longrightarrow H^+ + {}^\bullet OH \quad (7)$$

$$e^-_{(CB)} + O_2 \longrightarrow O_2^{\bullet-} \quad (8)$$

$$O_2^{\bullet-} + H^+ \longrightarrow HO_2^\bullet \quad (9)$$

$$2HO_2^\bullet + 2H^+ \longrightarrow H_2O_2 + 2{}^\bullet OH \quad (10)$$

$$2HO_2^\bullet \longrightarrow O_2 + H_2O_2 \quad (11)$$

$$H_2O_2 + e^-_{(CB)} \longrightarrow OH^- + {}^\bullet OH \quad (12)$$

Oxygen is required to produce $O_2^{\bullet-}$ and further oxidizing species by the interaction with solvent and H_2O_2 so the possible mechanism to convert target compound is going fast while at the anaerobic condition the possible mechanism to form oxidant only comes from the interaction between photon ($h\nu$) with solvent and homogeneous cleavage of OH bond of H_2O_2.

4. Conclusion

Iron immobilized TiO_2-montmorillonite (Fe/Ti-MMT) photocatalyst showed photoactivity in MB degradation by the photo-Fenton-like process. The photo-Fenton-like process obeyed the Elovich kinetic model. The model suggested that adsorption capability of the photocatalyst is important step in photodegradation mechanism.

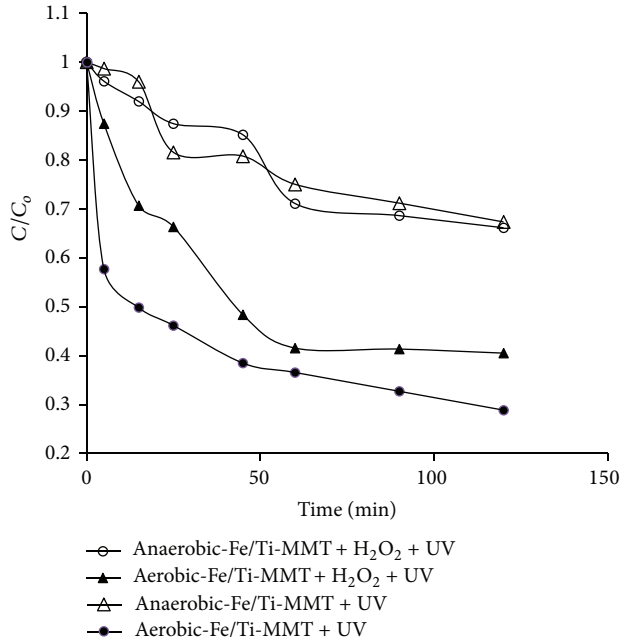

Figure 11: Photocatalysis and photooxidation of MB over Fe/Ti-MMT under aerobic and anaerobic condition (initial concentration = 5×10^{-4} M).

Conflict of Interests

The authors declare that there is no conflict of interests regarding the publication of this paper.

Acknowledgments

The authors thank DP2M-DIKTI for financial support to this research and also the Academic Development Board, Universitas Islam Indonesia, for supporting this publication.

References

[1] M. Lazar, S. Varghese, and S. Nair, "Photocatalytic water treatment by titanium dioxide: recent updates," *Catalysts*, vol. 2, no. 4, pp. 572–601, 2012.

[2] M. A. Quiroz, E. R. Bandala, and C. A. Martínez-Huitle, "Advanced Oxidation Processes (AOPs) for removal of pesticides from aqueous media," in *Pesticides—Formulations, Effects, Fate*, 2007.

[3] C. Gilmour, *Water treatment using advanced oxidation processes: application perspectives [M.S. thesis]*, University of Western Ontario, Ontario, Canada, 2012.

[4] A. Nickheslat, M. M. Amin, H. Izanloo, A. Fatehizadeh, and S. M. Mousavi, "Phenol photocatalytic degradation by advanced oxidation process under ultraviolet radiation using titanium dioxide," *Journal of Environmental and Public Health*, vol. 2013, Article ID 815310, 9 pages, 2013.

[5] P. Berdahl and H. Akbari, "Evaluation of titanium dioxide as a photocatalyst for removing air pollutants," CEC-500-2007-112, California Energy Commission, PIER Energy-Related Environmental Research Program, 2008.

[6] J. G. Carriazo, E. Guelou, J. Barrault, J. M. Tatibouët, and S. Moreno, "Catalytic wet peroxide oxidation of phenol over Al-Cu or Al-Fe modified clays," *Applied Clay Science*, vol. 22, no. 6, pp. 303–308, 2003.

[7] O. B. Ayodele, J. K. Lim, and B. H. Hameed, "Pillared montmorillonite supported ferric oxalate as heterogeneous photo-Fenton catalyst for degradation of amoxicillin," *Applied Catalysis A: General*, vol. 413-414, pp. 301–309, 2012.

[8] J. Kumar and A. Bansal, "Immobilization of nanoparticles of titanium dioxide for photocatalytic degradation," in *Proceedings of the International Conference on Future Trends in Structural, Civil, Environmental and Mechanical Engineering*, pp. 978–981, 2013.

[9] J.-W. Shi, "Preparation of Fe(III) and Ho(III) co-doped TiO_2 films loaded on activated carbon fibers and their photocatalytic activities," *Chemical Engineering Journal*, vol. 151, no. 1–3, pp. 241–246, 2009.

[10] J. Tokarský, L. Neuwirthová, P. Peikertová et al., "Polyaniline/TiO_2/kaolinite: the composite material with high electrical anisotropy," *Materials Chemistry and Physics*, vol. 146, no. 1-2, pp. 146–152, 2014.

[11] Y. Zhang, H. Gan, and G. Zhang, "A novel mixed-phase TiO_2/kaolinite composites and their photocatalytic activity for degradation of organic contaminants," *Chemical Engineering Journal*, vol. 172, no. 2-3, pp. 936–943, 2011.

[12] H. Yu, H. Irie, Y. Shimodaira et al., "An efficient visible-light-sensitive Fe(III)-grafted TiO_2 photocatalyst," *Journal of Physical Chemistry C*, vol. 114, no. 39, pp. 16481–16487, 2010.

[13] Q. Chen, P. Wu, Z. Dang et al., "Iron pillared vermiculite as a heterogeneous photo-Fenton catalyst for photocatalytic degradation of azo dye reactive brilliant orange X-GN," *Separation and Purification Technology*, vol. 71, no. 3, pp. 315–323, 2010.

[14] D. Chen, G. Du, Q. Zhu, and F. Zhou, "Synthesis and characterization of TiO_2 pillared montmorillonites: application for methylene blue degradation," *Journal of Colloid and Interface Science*, vol. 409, pp. 151–157, 2013.

[15] D. Chen, H. Zhu, and X. Wang, "A facile method to synthesize the photocatalytic TiO_2/montmorillonite nanocomposites with enhanced photoactivity," *Applied Surface Science*, vol. 319, pp. 158–166, 2014.

[16] I. Muthuvel, B. Krishnakumar, and M. Swaminathan, "Novel Fe encapsulated montmorillonite K10 clay for photo-Fenton mineralization of Acid Yellow 17," *Indian Journal of Chemistry A: Inorganic, Physical, Theoretical and Analytical Chemistry*, vol. 51, no. 6, pp. 800–806, 2012.

[17] S. K. Sahoo, K. Agarwal, A. K. Singh, B. G. Polke, and K. C. Raha, "Characterization of γ- and α-Fe_2O_3 nano powders synthesized by emulsion precipitation-calcination route and rheological behaviour of α-Fe_2O_3," *International Journal of Engineering, Science and Technology*, vol. 2, no. 8, pp. 118–126, 2010.

[18] J. T. Kloprogge, L. V. Duong, and R. L. Frost, "A review of the synthesis and characterisation of pillared clays and related porous materials for cracking of vegetable oils to produce biofuels," *Environmental Geology*, vol. 47, no. 7, pp. 967–981, 2005.

[19] L.-C. Chen, F.-R. Tsai, and C.-M. Huang, "Photocatalytic decolorization of methyl orange in aqueous medium of TiO_2 and Ag-TiO_2 immobilized γ-Al_2O_3," *Journal of Photochemistry and Photobiology A: Chemistry*, vol. 170, no. 1, pp. 7–14, 2005.

[20] K. Mondal and A. Sharma, "Photocatalytic oxidation of pollutant dyes in wastewater by TiO_2 and ZnO nano-materials—a mini-review," in *Nanoscience & Technology for Mankind*, pp. 36–72, 2014.

[21] W. Jo and R. J. Tayade, "Recent developments in photocatalytic dye degradation upon irradiation with energy-efficient light emitting diodes," *Chinese Journal of Catalysis*, vol. 35, no. 11, pp. 1781–1792, 2014.